Supplementary figures

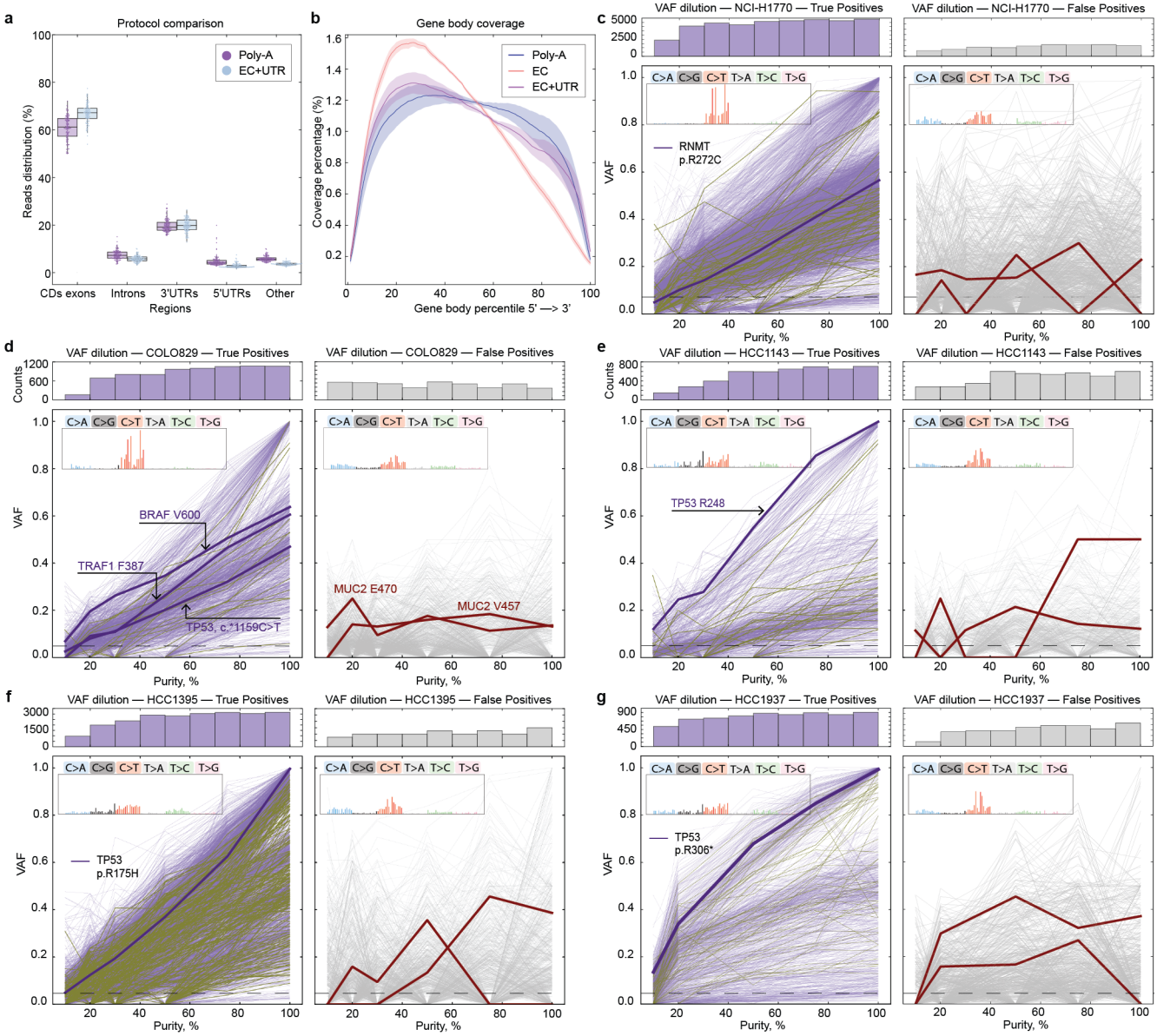

Supplementary Figure 1. Somatic mutation calling reference sets. a, Reads distribution for the optimized exome-capture (EC) protocol aligned with the poly-A seq protocol. **b**, Comparison of gene body coverage for different RNA capture protocols. **c-g**, VAF dilution from cell lines true positive SNVs (purple) and INDELs (brown) with 0.05 VAF limit of detection on the left plot. Stable number of error calls from each cell line for different purities on the right plot. Histogram represents the distribution of genomic contexts for identified mutations.

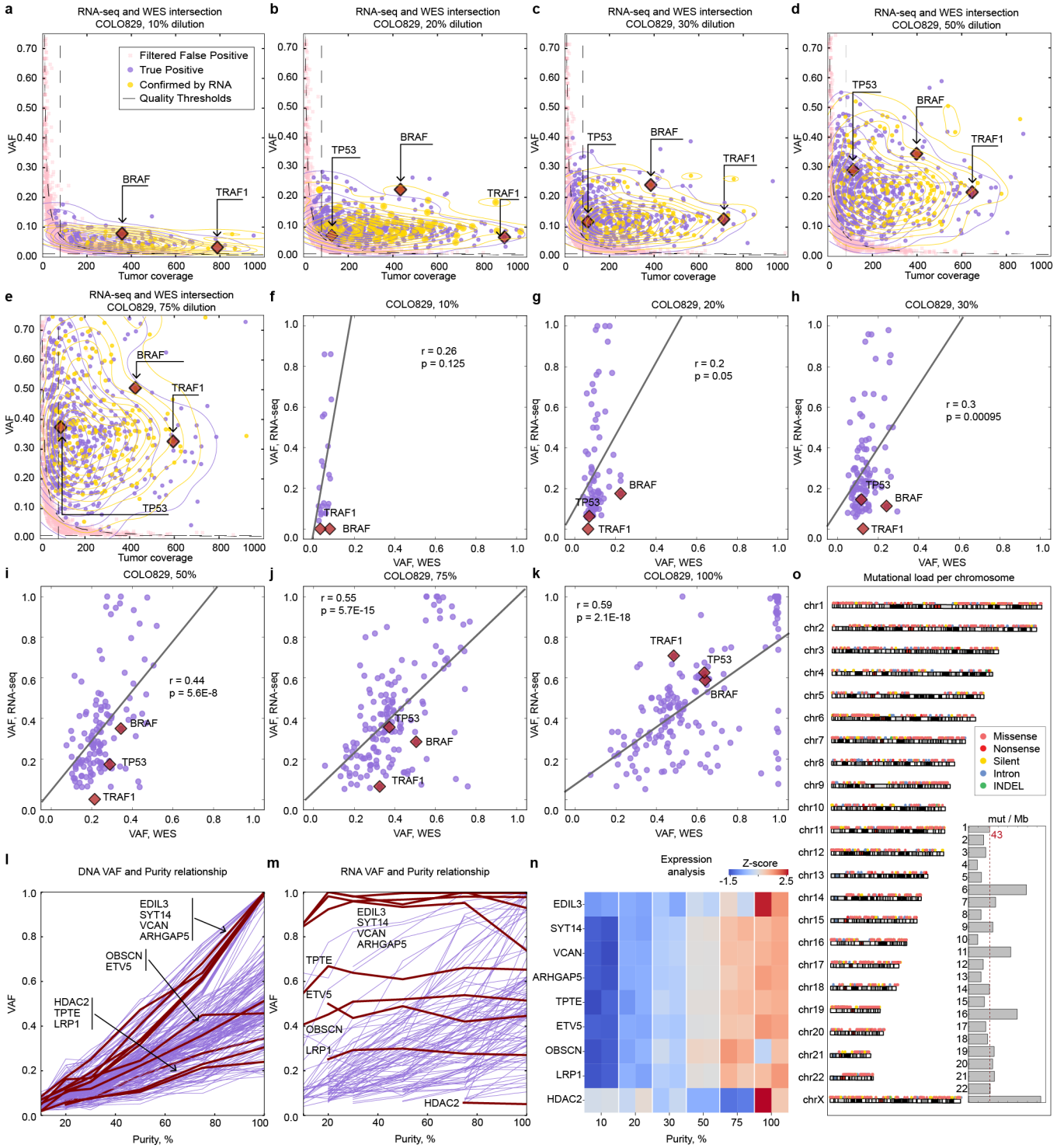

Supplementary Figure 2. Utilization of RNA-seq for somatic mutation calling. a-e, Scatter plot of VAF and coverage for all called variants in the COLO829 reference cell line for 10%, 30%, 50%, and 75% purities; true positives (purple) and RNA confirmed true positives (yellow). Dashed line indicates the threshold that filters false positives (red). **f-k**, Correlation of RNA and DNA VAF for a range of dilutions for the COLO829 cell line (10%, 20%, 30%, 50%, 75% and 100%). **l-m**, VAF of variants detected in WES (**l**) or RNA-seq (**m**) depending on the malignant cell purity of COLO829. Purple lines represent variants with concordant decrease in VAF relative to purity, while maroon lines indicate variants with non-decreasing VAF in RNA-seq across all dilutions. **n**, Heatmap showing gene expression levels for variants with non-decreasing VAF in RNA-seq across all dilutions. **o**, Distribution of created 3'042 reference variants across the human exome.

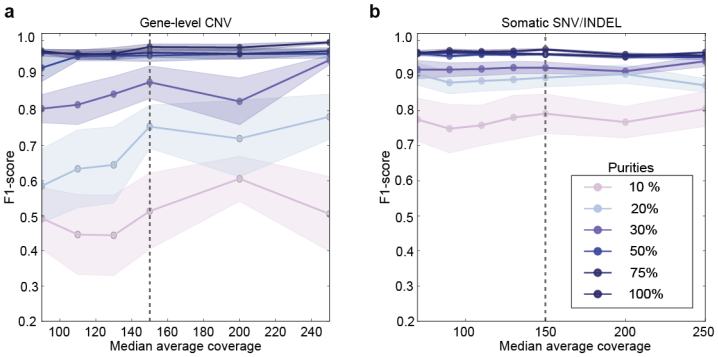

Supplementary Figure 3. Average coverage impact on performance characteristics. a-b, CNV (**a**) and somatic SNV/INDEL (**b**) mutation calling dependence on the median average coverage of the sample. Error ranges, s.e.m.

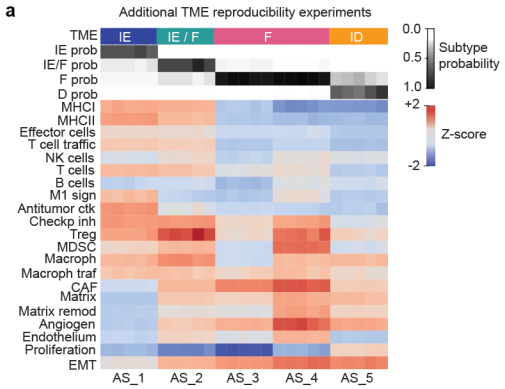

Supplementary Figure 4. TME reproducubility. a, Heatmap with gene signature scores from Bagaev et al. 40 across tested samples in all input amounts for additional inter-day reproducibility experiments for predicted TME subtypes.

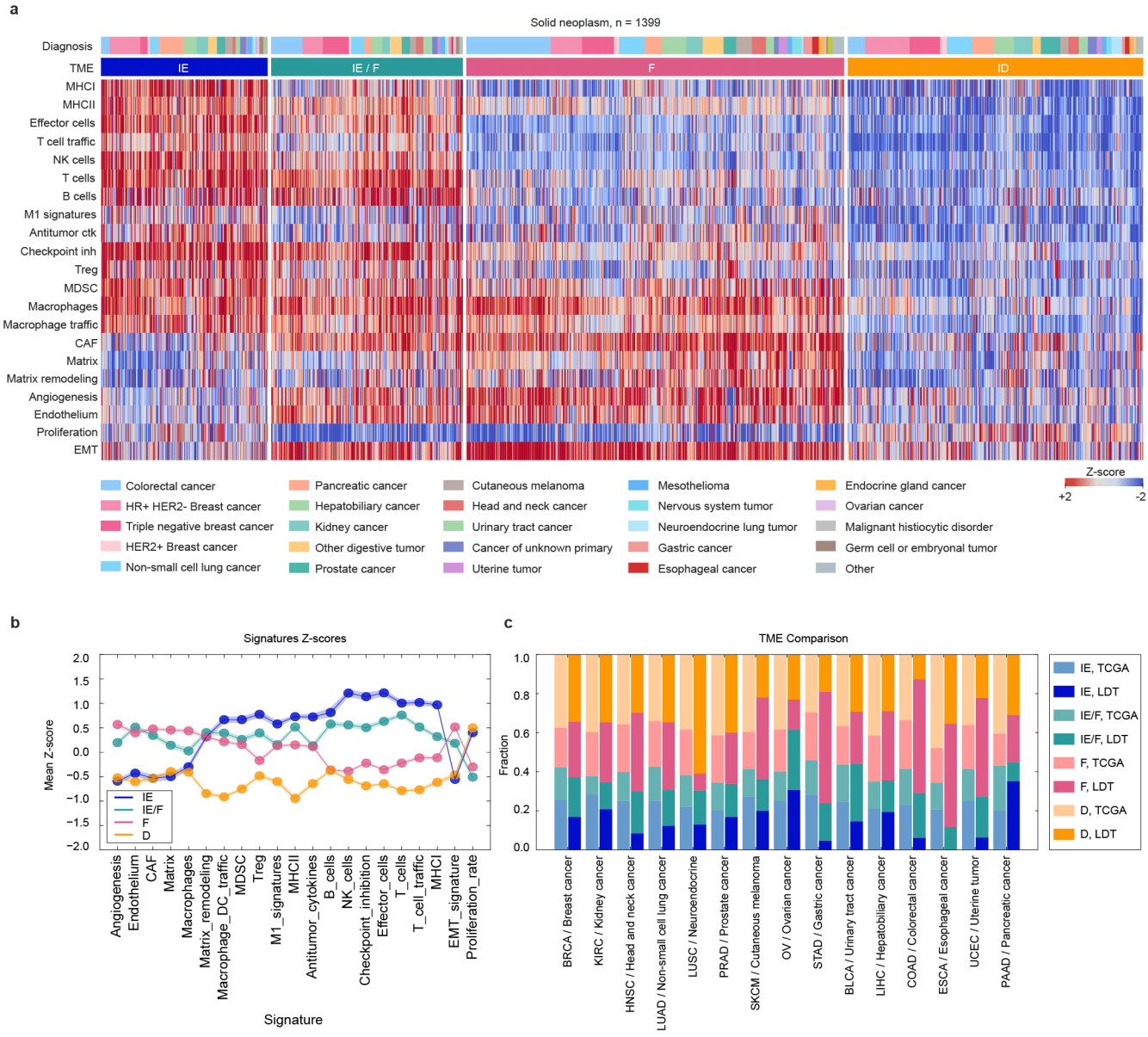

Supplementary Figure 5. TME clinical validation. a, Heatmap representing the distribution of ssGSEA scores for 21 signatures across all solid tumor samples (n = 1,399), grouped by TME subtype. **b**. Mean Z-score of 21 signatures calculated across all solid tumor samples (n = 1,399) used for TME classification. Error bars, s.e.m. **c**. Comparison of TME subtype distribution within cancer types between clinical samples and TCGA cohorts.

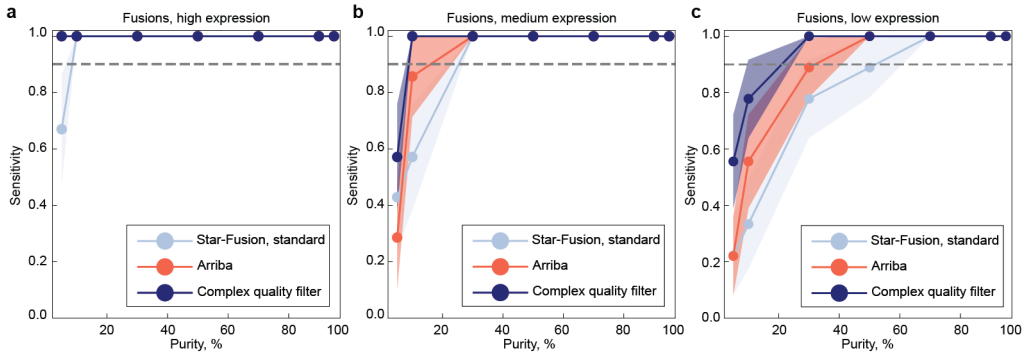

Supplementary Figure 6. Benchmark fusion calling pipelines. a-c, Comparison of sensitivity for fusion calling across range of tumor cell purity for compared fusion calling pipelines of high- (**a**), medium- (**b**) and low-expressed (**c**) fusions between widely used pipelines (Star-fusion recommended filters, Arriba) and (complex quality filter, adapted Star-fusion). Error ranges, s.e.m.

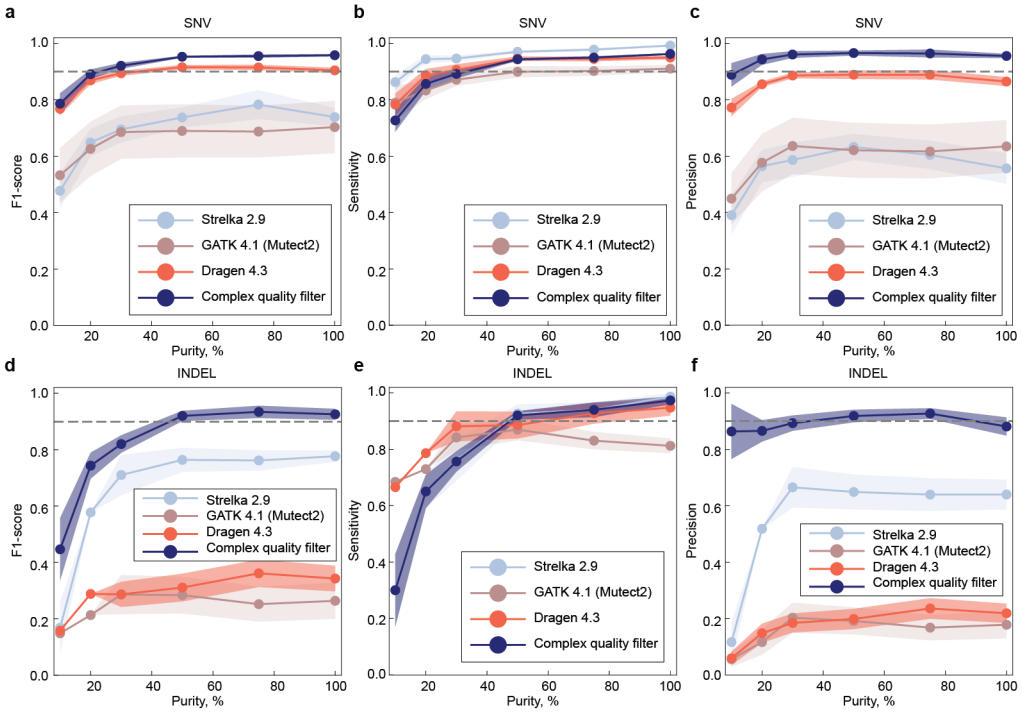

Supplementary Figure 7. Benchmark SNV/INDEL pipelines. a-f, Comparison of SNV (**a-c**) and Indel (**d-f**) F1-score, Sensitivity, and Precision between widely used pipelines (Strelka 2.9 recommended filters, GATK4.1, Dragen 4.3) and optimized pipeline (complex quality filter, adapted Strelka) across a range of tumor purities on reference cell lines. Error ranges, s.e.m.

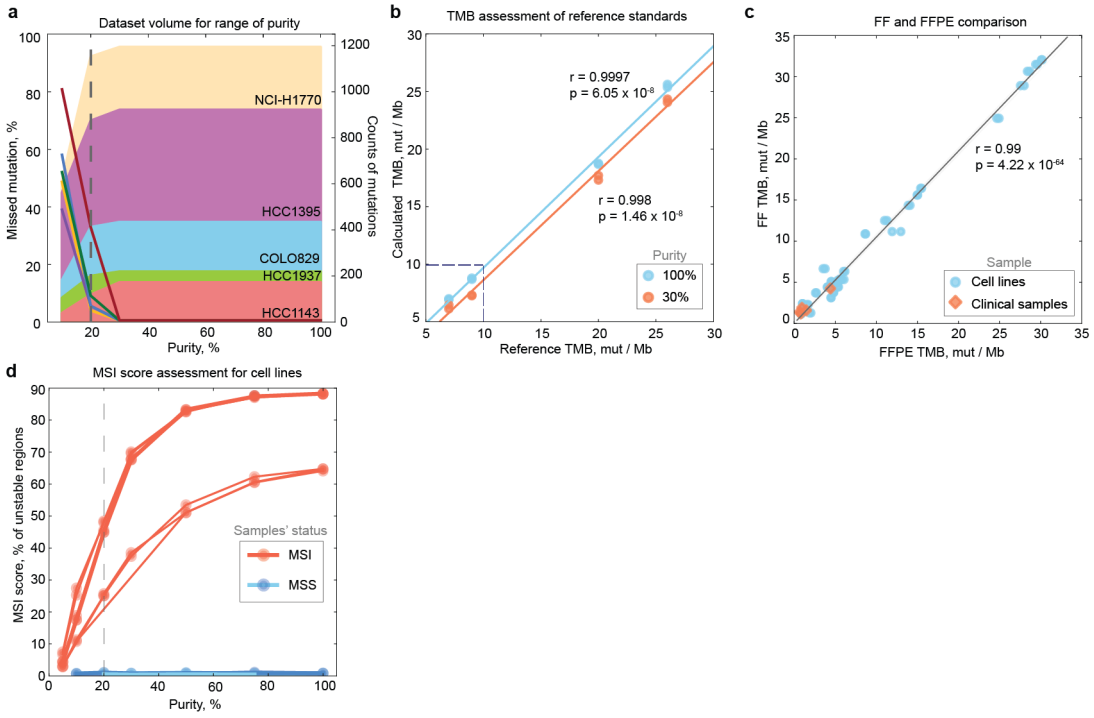

Supplementary Figure 8. Tumor Mutational Burden and MSI validation. a, Volume of corrected reference datasets for each cell line for a range of purities. Solid lines (red - HCC1143, blue - COLO829, yellow - NCI-H1770, green - HCC1937, purple - HCC1395) - proportion of lost mutations, % (left axis); **b**, Correlation of assessed TMB with SeraSeq reference TMB values for FF (100%) and FFPE (30%) reference materials (Pearson r = 0.99, n = 16). **c**, Correlation of FF and FFPE TMB scores across clinical samples and cell line references. **f**, Dependence of MSI score on tumor purity in cell line references. MSS - microsatellite stable, MSI - microsatellite instable.

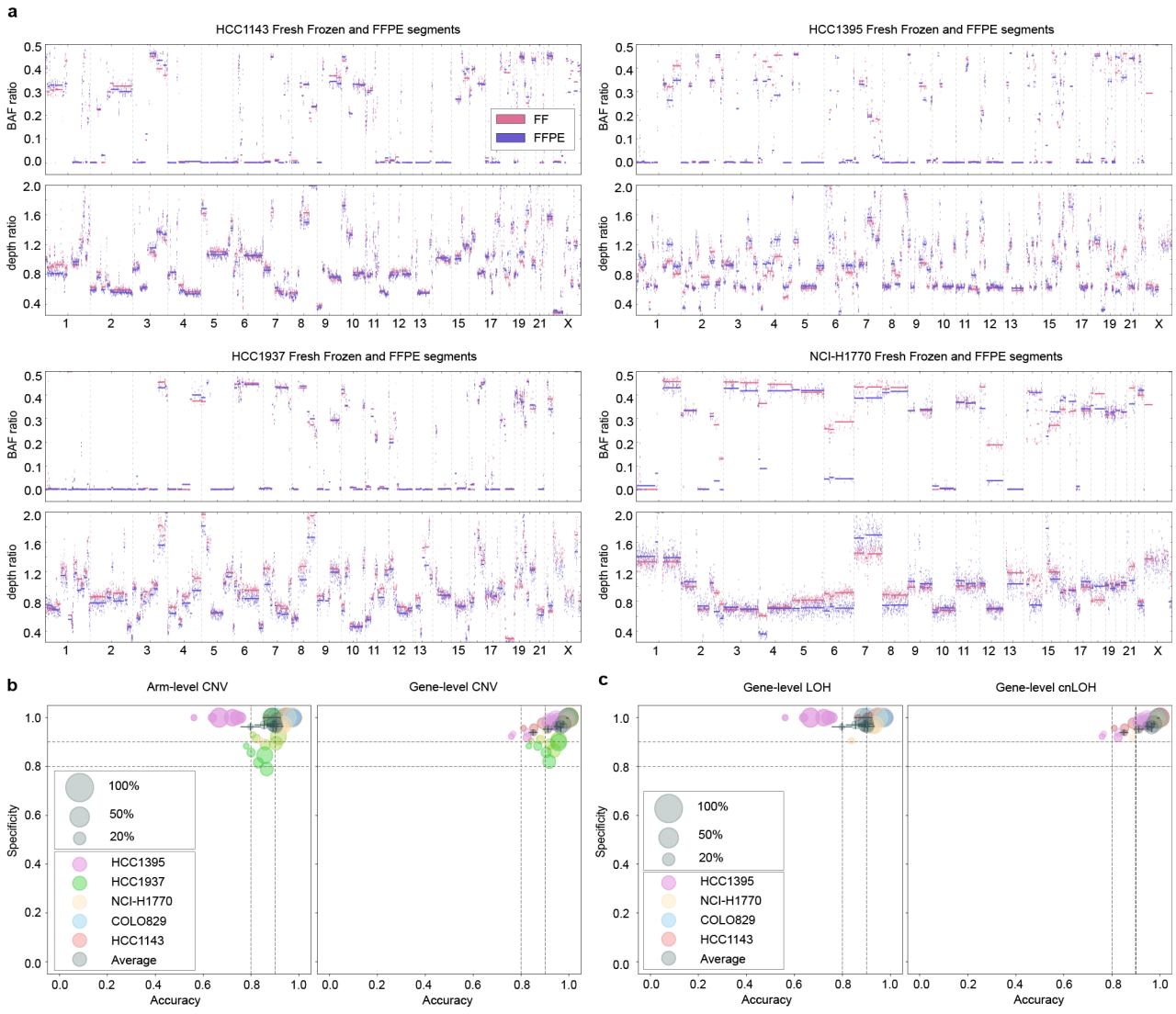

Supplementary Figure 9. Reference samples and performance characteristics for CNV calling. a, Comparison of reference exome for HCC1143, HCC1395, HCC1937, NCI-H1770 cell lines measured from FF or FFPE tissue. **b-c**, Arm- and gene-level CNV (**b**) and gene-level loss of heterozygosity (LOH) and copy-neutral LOH (cnLOH) (**c**) calling performance (additional metrics) across different purities for 5 reference cell lines. Error bars, s.e.m.

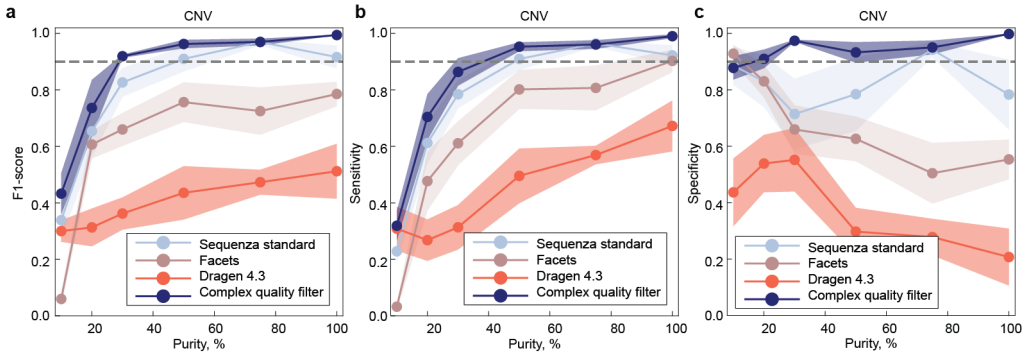

Supplementary Figure 10. Benchmark Copy Number Variant pipelines. a-c, F1-score, Sensitivity and Specificity of Copy Number Variant calling (all copies) between widely used pipelines (Sequenza recommended filters, Facets, Dragen 4.3) and pipeline presented in the work measured (complex quality filter, adapted Sequenza) on a reference cell lines across a wide range of tumor purity. Error ranges, s.e.m.

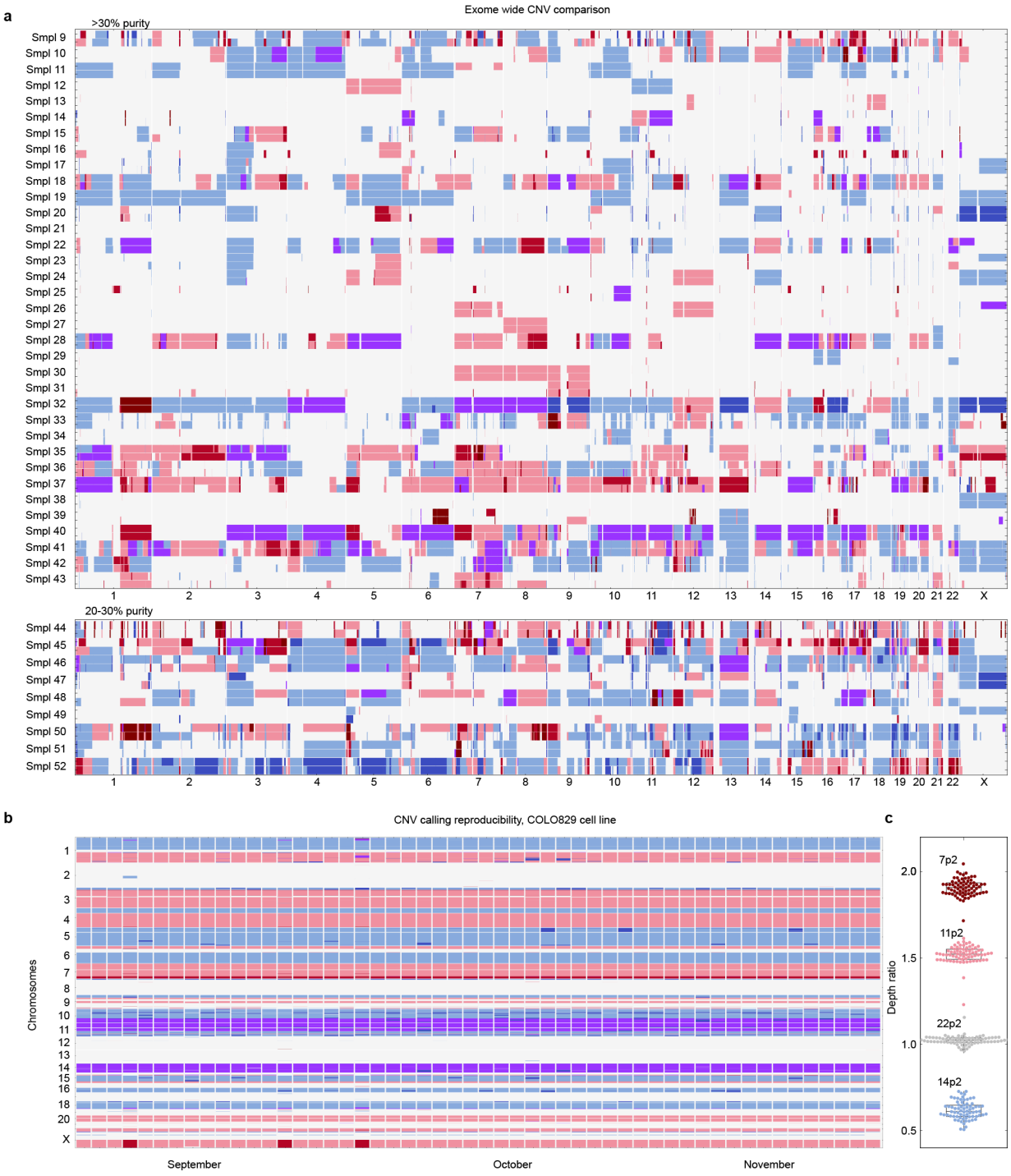

Supplementary Figure 11. Exome wide CNV profile comparison. a, Heatmaps representing exome-wide comparison of 44 clinical samples, sequenced in different laboratories; top - high purity samples, bottom - low purity samples. Gray - neutral, blue - shallow deletion, purple - deletion, pink - gain, red - amplification. **b**, Heatmap representing exome-wide comparison of COLO829 (internal control) samples over a 3-month period. **c,** Depth ratio for 4 segments of different status. Gray - neutral, blue - shallow deletion, purple - deletion, pink - gain, red - amplification.

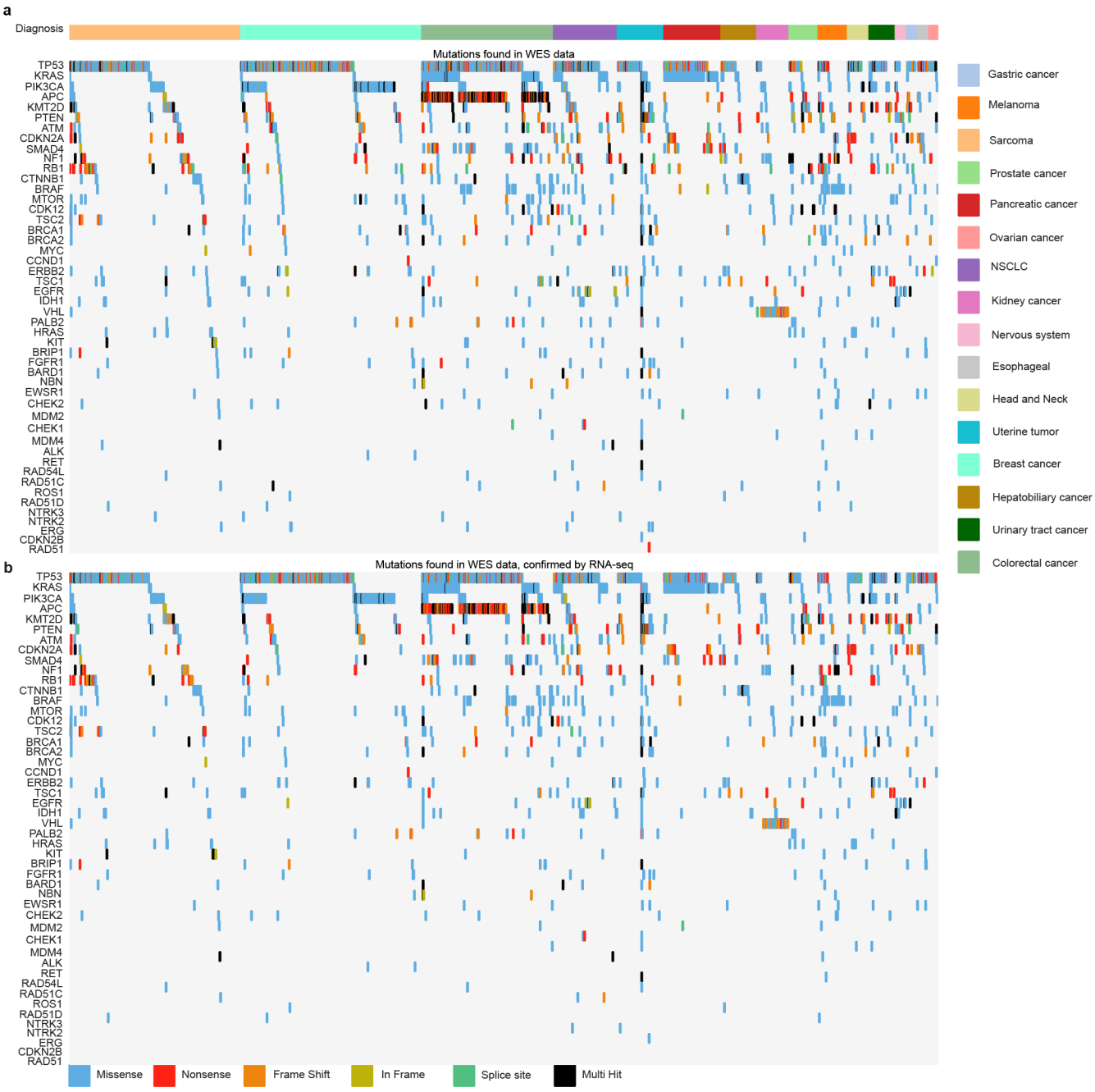

Supplementary Figure 12. RNA-seq and WES mutations. a-b, Side-by-side oncoplots for 2,230 patients with mutations identified from WES data (**a**) and RNA-seq confirmed mutations (**b**).

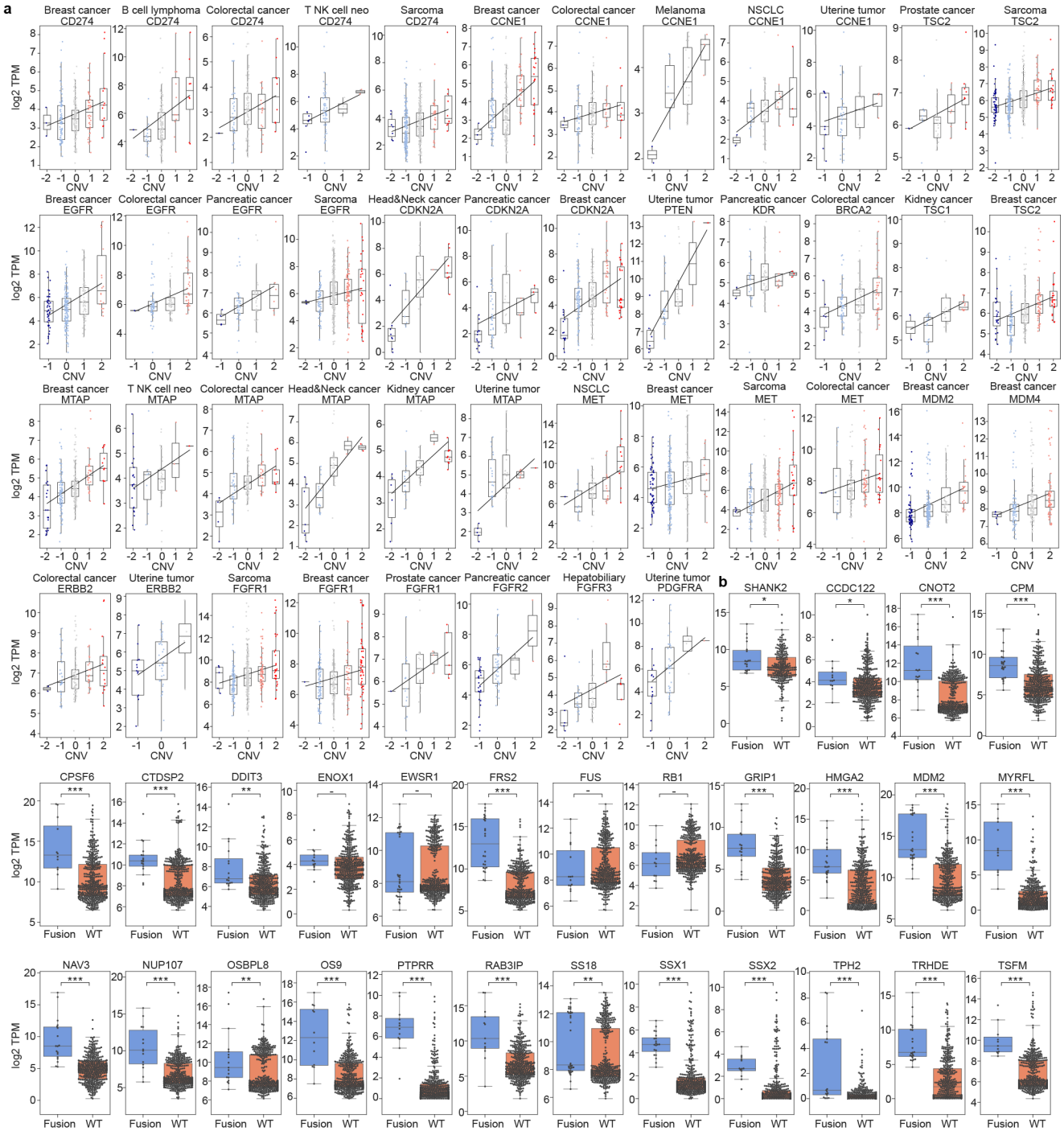

Supplementary Figure 13. RNA-seq integration for structural variants interpretation. a, Dependence of gene expression levels and CNV status for different genes. **b**, Partner gene expression levels in fusion partner genes for fusion-positive and –negative samples. **c**, Schema of driver fusion genes formation for TMPRSS2–ERG, DNAJB1–PRKACA.